

## Spontaneous Symmetry Breaking in Diffraction


J. Abad-Arredondo<sup>1</sup>, Z. Geng<sup>2</sup>, G. Keijsers<sup>2</sup>, F. Bijloo<sup>2</sup>, F. J. García-Vidal<sup>1,3</sup>,

A. I. Fernández-Domínguez<sup>1,\*</sup> and S. R. K. Rodríguez<sup>2,†</sup>

<sup>1</sup>*Departamento de Física Teórica de la Materia Condensada and Condensed Matter Physics Center (IFIMAC), Universidad Autónoma de Madrid, E28049 Madrid, Spain*

<sup>2</sup>*Center for Nanophotonics, AMOLF, Science Park 104, 1098 XG Amsterdam, The Netherlands*

<sup>3</sup>*Institute of High Performance Computing, Agency for Science, Technology, and Research (A\*STAR), Singapore*

 (Received 12 February 2024; revised 2 June 2024; accepted 19 August 2024; published 27 September 2024)

We demonstrate spontaneous symmetry breaking in the diffraction of a laser-driven grating with memory in its nonlinear response. We observe, experimentally and theoretically, asymmetric diffraction even when the grating and illumination are symmetric. Our analysis reveals how diffracted waves can spontaneously acquire momentum parallel to the lattice vector in quantities unconstrained by the grating period. Our findings point to numerous opportunities for imaging, sensing, and information processing with nonlinear periodic systems, which can leverage a much richer diffractive response than their linear counterparts.

DOI: [10.1103/PhysRevLett.133.133803](https://doi.org/10.1103/PhysRevLett.133.133803)

According to Bloch's theorem (BT), wave amplitudes in a periodic potential must have the same periodicity as the potential itself [1]. This basic property of waves stems from the relation between symmetries and conserved quantities unveiled by Noether [2]. Essentially, BT relies on the discrete translation symmetry of the system and the corresponding conservation of the wave vector component parallel to the lattice vector,  $k_{\parallel}$ . It may seem obvious that steady-state wave amplitudes must have the same symmetry as their confining potential. However, nature provides many counterexamples of this. Studies of spontaneous symmetry breaking (SSB) have shaped physics for decades [3]. For instance, the laser, Bose-Einstein condensation, superfluidity, superconductivity, the Josephson effect, and the Higgs boson, all emerge when a rotational U(1) symmetry is broken [4–6]. In addition, in atomic [7] and optical [8–15] systems, a mirror symmetry can spontaneously break and localized states with quantum entanglement can emerge [16,17]. In periodic systems, symmetry broken states have been theoretically analyzed [18], but not yet observed.

In this Letter, we demonstrate SSB in diffraction. We measure light scattering from a nonlinear grating with memory and, at sufficiently high intensities, we observe a cascade of dynamical effects in diffraction. These include spontaneous symmetry-breaking and symmetry-restoration transitions, as well as limit cycles and signatures of chaotic dynamics. Through numerical and analytical calculations at the level of Maxwell's equations, we explain our observations and elucidate how asymmetric diffraction can emerge from a symmetric system. Our approach extends the use of

linear stability analysis methods to extended photonic structures, and reveals how their refractive index fluctuation spectrum governs their behavior.

Figure 1(a) illustrates the system under study: a one-dimensional metallic grating coated with cinnamon oil. Placed on a glass substrate, it comprises aluminum [19] wires with 90 nm width, 70 nm height, and 366 nm lattice constant. A continuous wave laser impinges perpendicular to the periodicity plane. As detailed in Supplemental Material [20], its 532 nm wavelength is close to a grating resonance. Part of the laser light is absorbed by the oil, and then dissipated as heat. The resultant temperature rise causes the oil to expand, and its density and refractive index to decrease. This process, a thermo-optical nonlinearity, corresponds to an intensity-dependent refractive index. The refractive index change is time delayed by the oil's thermal relaxation, resulting in a nonlinear response with memory [22,23].

Figure 1(b) shows the sample's transmittance when modulating the laser power. The transmittance depends on the power and the direction of the power scan. This irreversibility, or hysteresis, is sometimes taken as an indication of bistability [24]: two stable states at a single driving condition. However, hysteresis can emerge without bistability [25,26]. A stronger evidence of bistability is the abrupt transmittance jump at 2.39 s, signaling a transition between states. The transmission versus input power plot [20], evidences a wide bistability region and an undershoot after the jump at 2.39 s. The half width at half maximum of the undershoot, 60  $\mu$ s, is indicative of the thermal relaxation time,  $\tau$  [22,23]. We also recorded images of the grating's reflection as a function of power. Figures 1(c)–1(e) show three images taken 50–70 ms after the jump. The bright disk and rings around the center of all images are due to the direct

\*Contact author: [a.fernandez-dominguez@uam.es](mailto:a.fernandez-dominguez@uam.es)

†Contact author: [s.rodriguez@amolf.nl](mailto:s.rodriguez@amolf.nl)

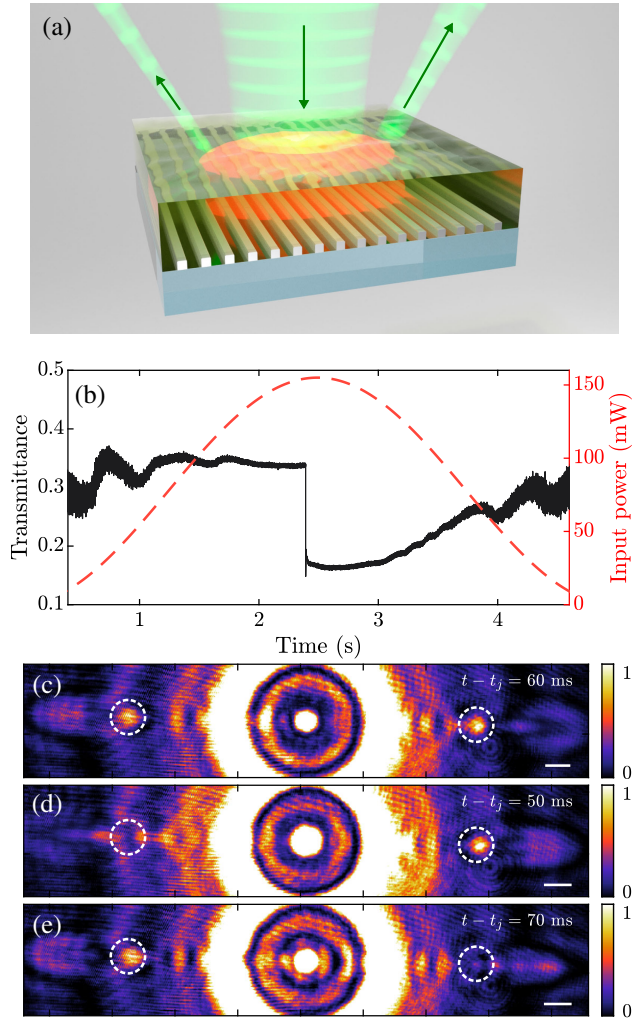


FIG. 1. (a) Oil-coated unblazed metallic grating, laser driven at normal incidence (not to scale). (b) Transmittance (solid curve) and input power (dashed curve) versus time, demonstrating optical bistability. (c)–(e) Reflection images recorded at  $t - t_j$  ms after the jump in transmittance observed at  $t_j = 2.4$  s in (b). Changes in +1 and -1 diffracted intensities (bright spots enclosed by dashed circles) evidence mirror SSB. Scale bar:  $3 \mu\text{m}$ .

laser reflection. The dots enclosed by dashed white circles are due to +1 and -1 diffraction orders [20].

The +1 and -1 diffracted intensities are similar in Fig. 1(c), but different in Figs. 1(d) and 1(e) which were taken 10 ms before and 10 ms after Fig. 1(c), respectively. Such differences in diffracted intensities emerged spontaneously in various scans. To investigate this effect with greater temporal resolution, we constructed a setup for isolating the two diffracted intensities (inside the dashed circles) from the background reflection and sending them to photodetectors [20]. The results are shown in Fig. 2, for the same modulation of the input power shown in Fig. 1(b). Purple and orange curves correspond to the -1 and +1 diffracted intensities,  $I_-$  and  $I_+$ , respectively.

Figure 2(a) displays rich dynamics of the diffracted intensities immediately after the jump, indicated by the

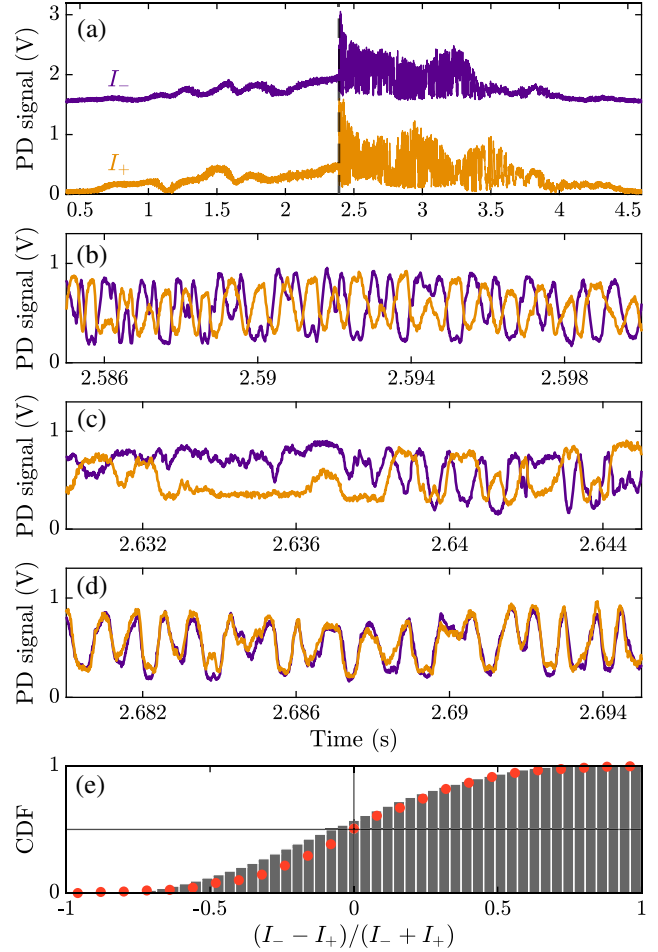


FIG. 2. (a) Diffracted intensities by the -1 (purple) and +1 (orange) orders, respectively, indicated by the dashed circles in Figs. 1(c)–1(e). The purple curve is displaced vertically for clarity. (b),(c),(d) are close-ups into intervals in (a) displaying out-of-phase oscillations, chaos, and in-phase oscillations, respectively. (e) Cumulative distribution functions for the intensity contrast between the -1 and +1 diffracted orders. Bars and red dots correspond to camera- and photodetector-acquired data, respectively.

vertical dashed black line. Figures 2(b)–2(d) show enlargements of three representative time windows, each 15 ms long. The rise in optical power during these 15 ms is much smaller than the standard deviation of the laser noise. Therefore, we can regard the average input power as constant. Figures 2(b) and 2(d) show out-of-phase and in-phase oscillations, respectively, of  $I_+$  and  $I_-$ . Such self-sustained oscillations, known as limit cycles [27], are here observed for the first time in diffraction. In between these two limit cycles, we observe a window of chaotic, uncorrelated dynamics as Fig. 2(c) shows.

The phase of a limit cycle is chosen spontaneously, similar to the spontaneous choice of the phase of a scalar field at a rotational  $U(1)$  symmetry breaking transition [6]. For this reason, limit cycles have drawn interest as manifestations of “time crystals”—self-organized periodic

states in time emerging through SSB [28–32]. Interestingly, the in-phase oscillations in Fig. 2(d) respect the mirror symmetry of the system, but the out-of-phase oscillations in Fig. 2(b) do not. This possibility, namely for mirror symmetry to be broken or not in a time crystalline phase, was recently analyzed in a model of coupled cavities [33]. Here, we evidence this phenomenon through power-induced mirror symmetry breaking and restoration.

Next, we assess whether symmetry breaking occurs spontaneously by fluctuations or deterministically by an unaccounted bias. Figures 1(c)–1(e) show indications of spontaneity: the  $-1$  and  $+1$  diffracted intensities imbalance spontaneously, with negligible change in power. Figure 2(d) shows indications of lack of bias: the two spontaneously synchronized trajectories have equal intensity. To go beyond qualitative indications, we analyzed the statistics of the contrast between diffraction intensities  $(I_- - I_+)/ (I_- + I_+)$ . Figure 2(e) shows the resultant cumulative distribution function (CDF) of the intensity contrast, measured with the photodetector and camera. We included data after the jump [dashed line in Fig. 2(a)], and up to the end of the dynamical regime (around 4 s). The CDFs contain data from multiple power scans and thus different noise realizations. Notice in Fig. 2(e) that both CDFs cross 0.5 near zero contrast, meaning intensity imbalances favoring the  $-1$  and  $+1$  orders are equally probable. The shape of both CDFs implies that symmetry is preserved on average, and unbroken most of the time. This can be observed more clearly in the corresponding probability distributions (see Supplemental Material [20]), which are symmetric and peaked at zero contrast. In Supplemental Material we further include a detailed discussion about the ( $\sim 100 \mu\text{s}$ ) timescale of SSB and the fluctuations triggering it [20].

Our experiments evidence mirror, but not discrete translation, SSB. The finite illumination area explicitly breaks translation symmetry. Actually, discrete translation SSB is impossible in experiments because the required single plane-wave illumination does not, strictly speaking, exist. Nonetheless, in Supplemental Material we demonstrate that the response of our grating is dominated by an approximate discrete translation symmetry [20]. Furthermore, to rigorously demonstrate discrete translation SSB in the idealized single plane-wave illumination case, we present next two complementary theoretical approaches based on Maxwell's equations. In both approaches, the oil layer is characterized by an intensity-dependent refractive index with memory:

$$n(\mathbf{r}, t) = n_0 - \gamma \int_{-\infty}^t ds K(t-s) |\mathbf{E}(\mathbf{r}, s)|^2. \quad (1)$$

$n_0$  is the linear refractive index,  $\gamma$  is the nonlinearity strength,  $\mathbf{E}(\mathbf{r}, t)$  is the electric field, and  $K(t) = e^{-t/\tau}/\tau$  is the same memory kernel used for oil-filled cavities [22,23].  $\tau$  is the thermal relaxation time of the oil, which is

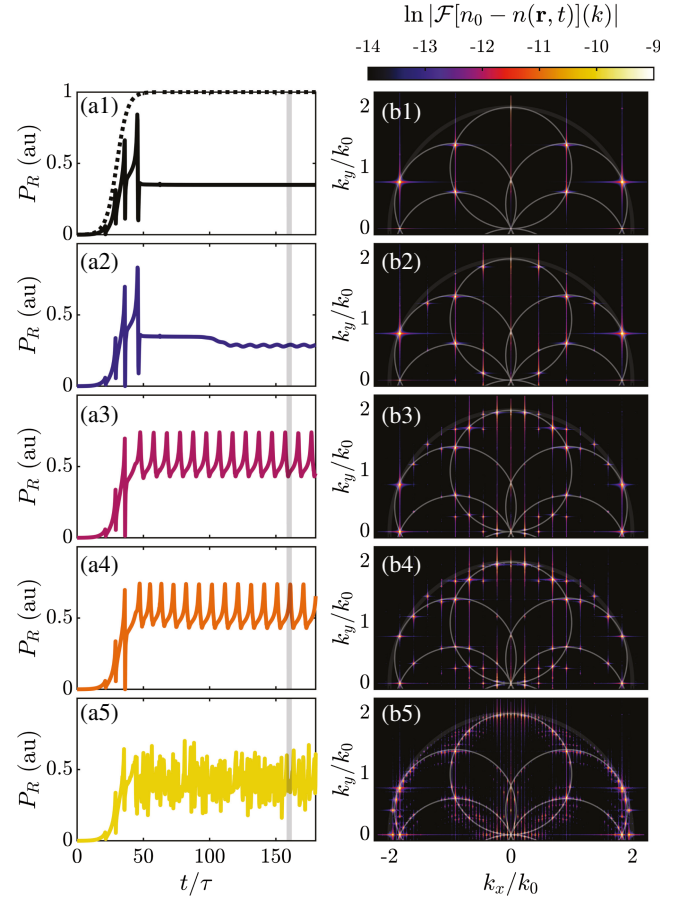


FIG. 3. (a) Calculated reflected power versus time. Panel numbers 1–5 correspond to supercell sizes of: 1, 2, 4, 8, and 16 grating periods, respectively. Dotted line in (a1) indicates the input power protocol. (b) Fourier transform, in natural log scale, of refractive index maps evaluated at the time indicated by the gray line in (a).

also the memory time of the system. We took all parameter values from experiments, and validated our model by reproducing the linear spectrum (see Supplemental Material [20]).

Our first approach involves full-wave simulations of nonlinear electromagnetic scattering under plane wave illumination. We solved for the electric fields in frequency domain as  $\mathbf{E}(\mathbf{r}, \omega, t)$  ( $t \sim \tau \gg 2\pi/\omega$ ). We avoided time-domain simulations by decoupling thermal and optical effects, which is justified for  $\tau \gg \Gamma^{-1}$  with  $\Gamma$  the optical dissipation rate;  $\tau/\Gamma^{-1} \sim 10^9$  in our experiments. We use mirror conditions on the lateral boundaries of the simulation domain. These are equivalent to Bloch periodic conditions for normal incidence and linear response but, unlike them, do not require *a priori* knowledge about parallel momentum components in the system [20].

Figures 3(a1)–3(a5) show the reflected power dynamics for a simulation domain containing 1, 2, 4, 8, and 16 grating periods, acting as a supercell. In all cases, the incident power increased as the dashed curve in Fig. 3(a1) shows.



For short times ( $t < 40\tau$ ), the reflection undergoes fast oscillations associated with the excitation of guided modes in the oil [20]. Afterwards, various dynamical regimes emerge depending on the supercell size. These include self-sustained oscillations with different periods as in Figs. 3(a2)–3(a4), and chaotic dynamics as in Fig. 3(a5). In Supplemental Material we show real-space refractive index maps at the time indicated by the vertical gray lines in Figs. 3(a1)–3(a5), evidencing local translation symmetry breaking. Using the same theoretical framework, we also qualitatively reproduce the experimentally observed optical hysteresis and elucidate its connection with SSB [20].

Figures 3(b1)–3(b5) show Fourier transforms of the refractive index maps,  $\mathcal{F}[n_0 - n(\mathbf{r}, t)]$ .  $k_0$  is the homogeneous medium wave vector. Most reciprocal space contributions fall on the thin circles of radius  $k_0$  centered at  $k_x = 0, \pm\pi/a$  and  $k_y = \sqrt{k_0^2 - k_x^2}$ , corresponding to wave vectors present in the linear solution. The thicker and fainter circle of radius  $2k_0$  encloses all wave vectors in  $n(\mathbf{r}, t)$  ( $\propto |\mathbf{E}|^2$ ) that are accessible by propagating plane waves. The peaks in Fig. 3(b1) all lie at  $k_{\parallel} = k_x = m2\pi/a$ , with  $m = 0, \pm 1, \pm 2$ , satisfying BT. In contrast, for larger supercells, wave vector contributions departing from BT emerge. In Supplemental Material we show that these wave vector components are responsible for the reflection oscillations in Figs. 3(a2)–3(a5), and thereby connect SSB in diffraction with the emergence of limit cycles in our system [20]. Figure 3(b5) shows a nearly homogeneous reciprocal-space peak density along the thin white circles, as expected for chaos. Our results show that mirror boundary conditions enable local translation SSB and self-sustained oscillations to emerge. However, the global inversion SSB responsible for the sudden change in the +1 and -1 diffracted intensities cannot occur under those boundary conditions.

To explain the emergence of asymmetric diffraction from a symmetric and symmetrically driven grating, we conceived a second approach using a Born scattering series to first order [34] and seeking a self-consistent solution to Maxwell's equations fed with Eq. (1). We treat the nonlinearity perturbatively, which is justified because the maximum modulation in the real-space refractive index maps associated with Fig. 3 is  $0.025 \ll 1.59 = n_0$  [20]. After a linearization technique described in Supplemental Material [20], we find that fluctuations to the refractive index map in reciprocal space,  $\delta n(\mathbf{k}, t) = \mathcal{F}[n(\mathbf{r}, t) - n_0]$ , satisfy

$$\tau \delta \dot{n}(\mathbf{k}, t) + \delta n(\mathbf{k}, t) = \frac{2\gamma E_0^2}{n_0 \chi} \sum_{\alpha\beta} M_{\alpha\beta}(\mathbf{k}) \delta n(\mathbf{k} + \mathbf{k}_\alpha - \mathbf{k}_\beta, t). \quad (2)$$

$\chi$  is the refractive index loss tangent (set according to experimental measurements),  $E_0$  is the incident plane wave amplitude,  $\alpha, \beta$  label the diffraction orders present in the

linear solution, and  $\delta \dot{n}(\mathbf{k}, t) = (d/dt)\delta n(\mathbf{k}, t)$ . The ratio  $\gamma E_0^2/\chi$  quantifies the balance between driving and dissipation, which determines the nonlinear threshold. The matrix  $M_{\alpha\beta}(\mathbf{k})$  (analytical expression in Supplemental Material [20]) describes the coupling between refractive index components of different wave vectors. It corresponds to the Jacobian determining the linear stability of a fixed point.  $M_{\alpha\beta}(\mathbf{k})$  diverges for  $\mathbf{k}$  at a distance  $k_0$  from the wave vectors of the linear solution. This condition indicates which reciprocal-space components beyond BT can emerge in  $n(\mathbf{r}, t)$ , and coincides with the thin white circles in Figs. 3(c1)–3(c5).

Equation (2) is nonlocal in reciprocal space, resulting in a complex interplay between different refractive index fluctuations. For instance, high-wave vector components excited by the evanescent fields at the metal grating can serve as a seed for fluctuations of arbitrary wave vectors. If the system crosses the nonlinear threshold, refractive index fluctuations that do not conserve momentum can be amplified and govern  $n(\mathbf{r}, t)$ . The properties of these fluctuations are determined by the eigenvalue problem  $\sum_{\alpha\beta} M_{\alpha\beta}(\mathbf{k}) \delta \tilde{n}_\lambda(\mathbf{k} + \mathbf{k}_\alpha - \mathbf{k}_\beta, t) = \lambda \delta \tilde{n}_\lambda(\mathbf{k}, t)$  corresponding to Eq. (2), and their dynamics satisfy  $\delta \tilde{n}_\lambda(\mathbf{k}, t) = \delta \tilde{n}_\lambda(\mathbf{k}, 0) \exp\{-[1 + (2\gamma E_0^2/n_0\chi)\lambda](t/\tau)\}$ . Defining a critical intensity  $E_c^2 = n_0\chi/2\gamma\text{Re}\{\lambda\}$ , a fluctuation is amplified or attenuated if  $E_0 > E_c$  or  $E_0 < E_c$ , respectively [35]. Therefore, refractive index fluctuations with the largest positive  $\text{Re}\{\lambda\}$  dominate the dynamics. Oscillatory dynamics are thus governed by  $\text{Im}\{\lambda\}$ , and, in agreement with our experiments, their period depends on  $\tau$  and incident power.

Figure 4 shows the eigenvalue spectrum of our system using different  $k$ -space discretizations corresponding to different supercell sizes, as in Fig. 3. Notice that eigenvalues belonging to larger supercell sizes coalesce along continuous curves, proving the convergence of the calculations against the  $k$ -space discretization. Figure 4(a) also shows that the maximum  $\text{Re}\{\lambda\}$  saturates for supercells larger than 16 grating periods, indicating that our results are representative of the continuum limit. The four governing eigenvalues in each case, with largest  $\text{Re}\{\lambda\}$ , are highlighted by white circles. Their real part increases, and therefore  $E_c$  diminishes, with supercell size, in agreement with the results in Fig. 3. The dominant eigenvalues are doubly degenerate in all cases (except for the single-period supercell), thereby allowing the system to reach any of the two associated eigenfunctions upon SSB.

Figure 4(b) illustrates the two eigenfunctions,  $\delta \tilde{n}_\lambda(\mathbf{k}, t)$ , (red and green dots) associated with the dominant degenerate eigenvalue for a 64 period supercell. We show the largest wave vector components only (amplitude encoded by the dot size) because the eigenfunctions are extremely pointed around a discrete set of wave vectors.  $k_x$  values allowed by momentum conservation are indicated by vertical dotted lines. Remarkably, the calculated dominant

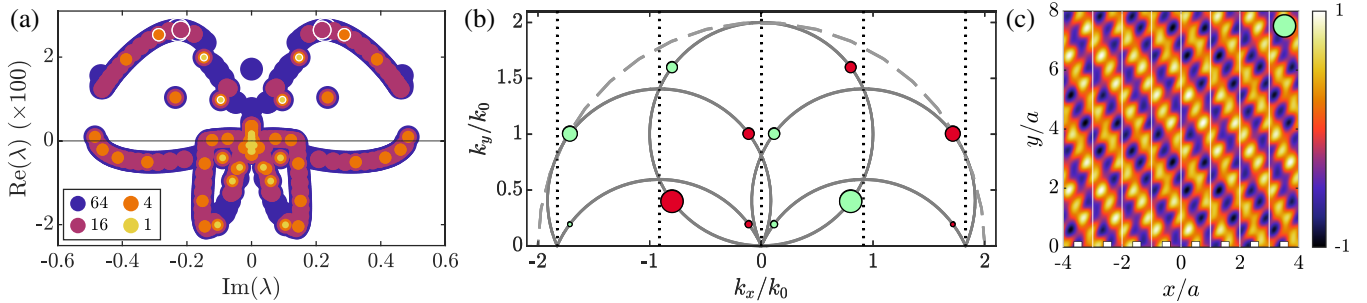


FIG. 4. (a) Eigenvalues  $\lambda$  for different imposed system periodicities. The four eigenvalues with the largest real part are highlighted with a white edge. (b) Reciprocal-space representation of the two (red and green) degenerate eigenfunctions,  $\delta\tilde{n}_\lambda(\mathbf{k}, t)$  with largest  $\text{Re}\{\lambda\}$  for 64 grating periods. Dot sizes encode eigenfunction amplitudes. Vertical dotted lines indicate wave vectors allowed by momentum conservation. (c) Real-space representation of the broken-symmetry eigenfunction plotted in green in (b).

wave vector contributions deviate from those lines, showcasing the breakdown of momentum conservation. Figure 4(c) renders one of the two degenerate eigenfunctions in real space, marked as green in Fig. 4(b), clearly breaking discrete translation symmetry. Above the non-linear threshold, fluctuations can lead the system into this or the other degenerate eigenfunction (its mirror image) via SSB. We observe this phenomenon for all supercell sizes exceeding one grating period, also in this model, indicating that our results hold in the continuum limit in  $k$  space.

To summarize, we have shown SSB in the diffraction of light from a nonlinear grating. Experimentally, we observed mirror SSB concomitantly with hysteresis, limit cycles, and chaotic dynamics in diffraction. Our results demonstrate that nonlinearity alone does not guarantee symmetry breaking. Actually, it can even restore mirror symmetry and trigger periodic solutions that comply with BT which assumes linearity. Our observations were reproduced by electromagnetic simulations and a linear stability analysis. These furthermore demonstrated how steady states with nonzero in-plane momentum can spontaneously emerge in perfectly periodic systems under normal plane-wave illumination, thereby breaking the discrete translation symmetry of the system. Our results open many opportunities for manipulating light without the constraints imposed by the symmetries of the system it interacts with. Taking advantage of recent advances in photonic materials and design maximizing light-matter interaction times [37], we foresee the implementation of stronger, faster, and tunable SSB phenomena in space and/or time in different areas. On one hand, SSB offers an unprecedented dynamical control over scattered light momenta and wave fronts which is promising for spatial light modulators and superresolution imaging [38]. On the other hand, SSB in spatially extended systems like ours can be exploited for biosensing applications which may require integration with microfluidics and without the need of nanophotonic field confinement [39]. Finally, by replacing our simple grating with more complex nanophotonic structures and illumination schemes, all-optical artificial neural networks for beyond von Neumann computing [40] may be realized.

*Acknowledgments*—We thank Femius Koenderink for discussions. This work is part of the research programme of the Netherlands Organisation for Scientific Research (NWO). S. R. K. R. acknowledges an ERC Starting Grant with Project No. 852694. J. A.-A., A. I. F.-D., and F. J. G.-V. acknowledge funding from the Spanish Ministry of Science, Innovation and Universities through Grant No. PID2021-126964OB-I00, No. PID2021-125894NB-I00, and No. TED2021-130552B-C21, as well as the European Union’s Horizon Programme through Grant No. 101070700 (MIRAQLS).

- [1] F. Bloch, *Z. Phys.* **52**, 555 (1929).
- [2] E. Noether, *Math. Klasse* **1918**, 235 (1918), <https://eudml.org/doc/59024>.
- [3] P. W. Anderson, *Science* **177**, 393 (1972).
- [4] M. Endres, T. Fukuhara, D. Pekker, M. Cheneau, P. Schauß, C. Gross, E. Demler, S. Kuhr, and I. Bloch, *Nature (London)* **487**, 454 (2012).
- [5] N. Navon, A. L. Gaunt, R. P. Smith, and Z. Hadzibabic, *Science* **347**, 167 (2015).
- [6] A. Beekman, L. Rademaker, and J. van Wezel, *SciPost Phys. Lect. Notes* **11** (2019).
- [7] T. Zibold, E. Nicklas, C. Gross, and M. K. Oberthaler, *Phys. Rev. Lett.* **105**, 204101 (2010).
- [8] *Spontaneous Symmetry Breaking, Self-Trapping, and Josephson Oscillations*, edited by B. A. Malomed, *Progress in Optical Science and Photonics Vol. 1* (Springer Berlin Heidelberg, Berlin, Heidelberg, 2013), p. 707, [10.1007/978-3-642-21207-9](https://doi.org/10.1007/978-3-642-21207-9).
- [9] P. Hamel, S. Haddadi, F. Raineri, P. Monnier, G. Beaudoin, I. Sagnes, A. Levenson, and A. M. Yacomotti, *Nat. Photonics* **9**, 311 (2015).
- [10] Q.-T. Cao, H. Wang, C.-H. Dong, H. Jing, R.-S. Liu, X. Chen, L. Ge, Q. Gong, and Y.-F. Xiao, *Phys. Rev. Lett.* **118**, 033901 (2017).
- [11] B. Garbin, J. Fatome, G. L. Oppo, M. Erkintalo, S. G. Murdoch, and S. Coen, *Phys. Rev. Res.* **2**, 023244 (2020).
- [12] G. Xu, A. U. Nielsen, B. Garbin, L. Hill, G.-L. Oppo, J. Fatome, S. G. Murdoch, S. Coen, and M. Erkintalo, *Nat. Commun.* **12**, 4023 (2021).

- [13] B. Garbin, A. Giraldo, K. J. H. Peters, N. G. Broderick, A. Spakman, F. Raineri, A. Levenson, S. R. K. Rodriguez, B. Krauskopf, and A. M. Yacomotti, *Phys. Rev. Lett.* **128**, 053901 (2022).
- [14] A. Krasnok and A. Alù, *ACS Photonics* **9**, 2 (2022).
- [15] L. Hill, G.-L. Oppo, and P. Del’Haye, *Commun. Phys.* **6**, 208 (2023).
- [16] A. Micheli, D. Jaksch, J. I. Cirac, and P. Zoller, *Phys. Rev. A* **67**, 013607 (2003).
- [17] W. Casteels and C. Ciuti, *Phys. Rev. A* **95**, 013812 (2017).
- [18] P. A. Kalozoumis, C. Morfonios, F. K. Diakonou, and P. Schmelcher, *Phys. Rev. Lett.* **113**, 050403 (2014).
- [19] A. D. Rakić, *Appl. Opt.* **34**, 4755 (1995).
- [20] See Supplemental Material at <http://link.aps.org/supplemental/10.1103/PhysRevLett.133.133803> for measurements and simulations of the linear spectrum of the grating, finite size simulations demonstrating the origin of the diffracted orders in Fig. 1, details about the experimental setup and the statistical analysis demonstrating SSB experimentally, real space maps of the symmetry-broken refractive index profile, limit cycles, linking of limit cycles to SSB, theoretical reproduction of the hysteresis phenomena, derivation of linear stability analysis method, numerical implementation details, and Ref. [21].
- [21] V. G. Ramesh, K. J. H. Peters, and S. R. K. Rodriguez, *Phys. Rev. Lett.* **132**, 133801 (2024).
- [22] Z. Geng, K. J. H. Peters, A. A. P. Trichet, K. Malmir, R. Kolkowski, J. M. Smith, and S. R. K. Rodriguez, *Phys. Rev. Lett.* **124**, 153603 (2020).
- [23] K. J. H. Peters, Z. Geng, K. Malmir, J. M. Smith, and S. R. K. Rodriguez, *Phys. Rev. Lett.* **126**, 213901 (2021).
- [24] G. A. Wurtz, R. Pollard, and A. V. Zayats, *Phys. Rev. Lett.* **97**, 057402 (2006).
- [25] F. Broner, G. H. Goldsztein, and S. H. Strogatz, *SIAM J. Appl. Math.* **57**, 1163 (1997).
- [26] S. R. K. Rodriguez, W. Casteels, F. Storme, N. Carlon Zambon, I. Sagnes, L. Le Gratiet, E. Galopin, A. Lemaître, A. Amo, C. Ciuti, and J. Bloch, *Phys. Rev. Lett.* **118**, 247402 (2017).
- [27] S. H. Strogatz, *Nonlinear Dynamics and Chaos With Applications to Physics, Biology, Chemistry, and Engineering* (CRC Press, Boca Raton, 2018), pp. 1–513, 10.1201/9780429492563.
- [28] A. Shapere and F. Wilczek, *Phys. Rev. Lett.* **109**, 160402 (2012).
- [29] D. V. Else, C. Monroe, C. Nayak, and N. Y. Yao, *Annu. Rev. Condens. Matter Phys.* **11**, 467 (2020).
- [30] M. Marconi, F. Raineri, A. Levenson, A. M. Yacomotti, J. Javaloyes, S. H. Pan, A. E. Amili, and Y. Fainman, *Phys. Rev. Lett.* **124**, 213602 (2020).
- [31] P. Kongkhambut, J. Skulte, L. Mathey, J. G. Cosme, A. Hemmerich, and H. Keßler, *Science* **377**, 670 (2022).
- [32] T. L. Heugel, A. Eichler, R. Chitra, and O. Zilberberg, *SciPost Phys. Core* **6**, 053 (2023).
- [33] C. Lledó and M. H. Szymańska, *New J. Phys.* **22**, 075002 (2020).
- [34] L. Novotny and B. Hecht, *Principles of Nano-Optics*, 2nd ed. (Cambridge University Press, Cambridge, England, 2012), Vol. 9781107005, pp. 1–564, 10.1017/CBO9780511794193.
- [35] Note that this threshold is derived upon the assumption that the nonlinear medium extends infinitely. It should therefore be taken as a lower bound of the nonlinear threshold in the finite, experimental system [36].
- [36] R. Hoyle, *Pattern Formation: An Introduction to Methods* (Cambridge University Press, UK, 2006), 10.1017/CBO9780511616051.
- [37] J. B. Khurgin, *Nat. Photonics* **17**, 545 (2023).
- [38] A. Forbes, M. de Oliveira, and M. R. Dennis, *Nat. Photonics* **15**, 253 (2021).
- [39] H. Altug, S.-H. Oh, S. A. Maier, and J. Homola, *Nat. Nanotechnol.* **17**, 5 (2022).
- [40] X. Lin, Y. Rivenson, N. T. Yardimci, M. Veli, Y. Luo, M. Jarrahi, and A. Ozcan, *Science* **361**, 1004 (2018).